ACS Biomaterials SCIENCE & ENGINEERING
Article
Cite This: ACS Biomater. Sci. Eng. XXXX, XXX, XXX−XXX

Silk Fibroin Porous Scaffolds Loaded with a Slow-Releasing Hydrogen Sulfide Agent (GYY4137) for Applications of Tissue Engineering

Rosasilvia Raggio,[†,‡,#] Walter Bonani,[†,‡,#] Emanuela Callone,[†,§] Sandra Dirè,[†,§] Laura Gambari,[∥] Francesco Grassi,*[,∥] and Antonella Motta*[,†,‡]

[†]Department of Industrial Engineering, University of Trento, Via Sommarive 9, 38123 Trento, Italy

[‡]BIOtech Research Center and European Institute of Excellence on Tissue Engineering and Regenerative Medicine, Via delle Regole 101, 38123 Trento, Italy

[§]"Klaus Muller" Magnetic Resonance Laboratory, Department of Industrial Engineering, University of Trento, Via Sommarive 9, 38123 Trento, Italy

[∥]RAMSES Laboratory, IRCCS Istituto Ortopedico Rizzoli, Via di Barbiano 1/10, 40136 Bologna, Italy

ABSTRACT: Hydrogen sulfide (H_2S) is a physiological gasotransmitter known to possess a regulatory role in several tissues, including bone. The exogenous administration by injection of solutions of H_2S-releasing compounds (e.g., GYY4137) has been previously investigated as a novel therapeutic approach for the treatment of bone diseases. Here, GYY4137 was embedded into fibroin sponges, previously shown to be suitable as scaffolds for bone, thanks to their biocompatibility, scalable porous structure, and biodegradability rate. Fibroin porous scaffolds were produced by solvent casting and the particulate leaching method, and GYY4137 was successively incorporated by using dimethyl sulfoxide (DMSO) as vehicle. The process used to produce GYY4137-loaded scaffolds allowed the incorporation of different controlled amounts of GYY4137 into fibroin matrices. The loading process preserved the properties of the system components in the final products, as assessed by SEM, FT-IR, NMR, and different thermal analyses techniques. Release of H_2S from GYY4137 incorporated into the scaffolds was monitored upon incubation in saline solution at physiological pH: H_2S-release kinetic was found to be dependent on the amount of GYY4137. To ensure biocompatibility, mouse fibroblasts and human primary bone marrow stromal cells were seeded onto scaffolds, and short-term viability assays were performed. Results showed that the GYY4137-loaded scaffold did not induce cytotoxicity in any of the cell type tested. Our findings demonstrate that embedding an H_2S-releasing donor in silk fibroin scaffold is a suitable strategy to achieve a long-lasting release of H_2S that preserves cell viability and allows local delivery at sites of tissue injury.

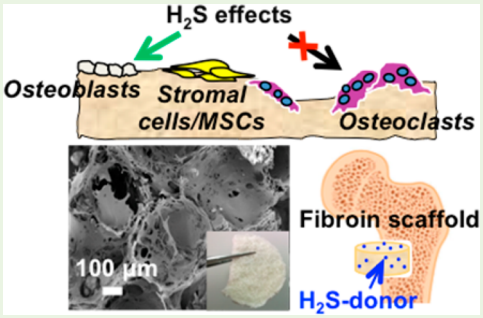

KEYWORDS: *hydrogen sulfide, GYY4137, silk fibroin, scaffold, bone tissue engineering*

INTRODUCTION

Hydrogen sulfide (H_2S) is known to be physiologically present in mammalian tissues, produced in nanomolar concentrations by cells, and is nowadays included in the family of the endogenous gaseous messenger molecules, or gasotransmitters, together with nitric oxide (NO) and carbon monoxide (CO).[1] The most relevant source of endogenous H_2S is generated from the amino acid L-cysteine by the combined catalytic activity of the enzymes cystathionine β-synthase (CBS) and cystathionine γ-lyase (CSE), both involved in methionine and in dietary cysteine metabolic pathways.[2]

In the last 20 years, starting from the discoveries of Abe and Kimura in 1996,[3] concentration levels of H_2S in different tissues have been investigated, and some of its biochemical and molecular processes have been clarified, providing scientists the opportunity to appreciate it as an essential ubiquitous modulator in the homeostasis of various tissues and organs, such as the brain, blood vessels, and the gastrointestinal tract.[3−5] The biological role of H_2S also extends to bone development and function. It was shown that exogenous H_2S, in concentrations ranging between 50 and 200 μmol/L, stimulated osteogenesis from human bone marrow stromal cells (hMSCs), by controlling Ca^{2+} influx through their ion channels, and dose-dependently inhibited human osteoclasts (hOCs) differentiation and function, as revealed by the capability to break down a mineral substrate.[6,7]

These findings suggest that exogenously administered H_2S, may have a therapeutic role in the treatment of bone diseases, such as fractures, bone loss, and erosion due to injuries, osteoporosis, and complications due to surgical operations.[7,8]

Two of the most commonly used donors of H_2S are sodium hydrosulfide (NaHS) and (*p*-methoxyphenyl)morpholino-

Received: February 22, 2018
Accepted: July 6, 2018
Published: July 6, 2018

DOI: 10.1021/acsbiomaterials.8b00212
ACS Biomater. Sci. Eng. XXXX, XXX, XXX−XXX

phosphinodithioic acid (GYY4137). In particular, GYY4137 possesses a relatively slow H_2S-release kinetic compared to NaHS, making it more suitable for the exogenous administration of H_2S in *in vitro* and *in vivo* experiments.[9,10] Previous works reported that GYY4137 decomposes by hydrolysis, releasing low amounts of soluble H_2S gas in aqueous solution over a sustained period of time, in a temperature and pH-dependent manner.[11] Moreover, H_2S release from GYY4137 was shown to be a L-cysteine-activated mechanism, meaning that, in the presence of a biological thiol, such as L-cysteine, H_2S release became significant, nevertheless remaining slow and prolonged.[12,13]

In previously published studies, GYY4137 was administered systemically by injection to regulate, restore, and maintain H_2S concentration levels in solution in *in vitro* experiments, or in tissues and biological fluids in *in vivo* conditions.[8,11,14−16] To the best of our knowledge, a 3D system to achieve localized and sustained release of H_2S has not been explored before.

The aims of the present study were the realization and the characterization of an engineered scaffold combined with GYY4137, and the evaluation of its ability to provide a local release of H_2S in a biologic environment. These steps of preliminary validation are mandatory prior to evaluate the scaffold-dependent properties in inducing bone formation.

Various materials and fabrication techniques have been employed for the production of scaffolds for bone tissue engineering.[17] Among the material sources, silkworm cocoons have been extensively exploited for the extraction of silk fibroin (SF), the structural protein constituting the core of silk fibers. In fact, fibroin was successfully used as suture material for centuries and is nowadays appreciated to form biomaterials for different medical uses.[18] Starting from SF aqueous solutions and using simple, environmentally safe, and low-cost processing routes, various SF-based constructs and 3D frameworks could be prepared.[19] The protein conformation, the crystallinity and the morphology conferred on SF during the fabrication of the biomaterial have a strong impact on the biological properties. In particular, 3D SF-based porous constructs, produced by salt leaching, demonstrated great biocompatibility as scaffolds for bone tissue engineering, thanks to the ability to enhance cell attachment, proliferation, and migration, the biodegradability properties, and the morphology, in terms of quality and degree of porosity.[20−24] In different experiments, SF scaffolds were shown to be osteoconductive, by promoting *in vitro* osteogenesis in a range of bone-related cell types,[25−28] and supporting the formation of new bone tissue when implanted *in vivo*.[29,30] In addition, thanks to the stability and the flexibility of these materials, various modifications of SF scaffolds have been generated with chemical, structural, and biological innovations, or they were successfully combined with various bioactive agents and growth factors,[31−33] with the final goal of enhancing the osteoinductive properties and the regenerative potentials.

Starting from this evidence, this manuscript describes a novel type of SF scaffold loaded with the H_2S donor GYY4137, intended to operate as H_2S releasing system to be used in the near future in bone regeneration studies. With this goal, highly porous silk fibroin matrices were produced by salt leaching. Then, the scaffolds were loaded postfabrication with different amounts of GYY4137, in order to explore the effects of different concentration of the H_2S donor on the properties, the H_2S releasing abilities, and the cytotoxicity of the final products.

MATERIALS AND METHODS

Materials. H_2S donor GYY4137 (M_w = 376.47 g/mol) was purchased from Cayman Chemical (Ann Arbor, MI, U.S.A.). GYY4137 was supplied as the morpholinium salt of (*p*-methoxyphenyl)morpholino-phosphinodithioic acid, a white crystalline solid (Figure 1).

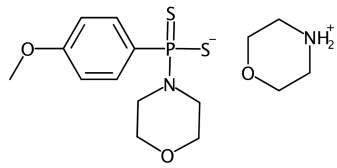

Figure 1. Structural formula of the H_2S donor GYY4137.

Anhydrous dimethyl sulfoxide (DMSO), lithium bromide (LiBr), sodium carbonate (Na_2CO_3), and sodium chloride (NaCl) were purchased from Sigma-Aldrich (Saint Louis, MO, U.S.A.).

Bombyx mori cocoons (purchased from Chul Thai Silk Co., Phetchabun, Thailand) were used as source of SF.

Preparation of SF Aqueous Solution. Silk cocoons were degummed by two consecutive treatments with Na_2CO_3 aqueous solutions, at a concentration of 1.1 and 0.4 g/L, respectively, at 98 °C for 1.5 h each time. The fibers obtained were deeply rinsed with deionized (DI) water and then air-dried. Degummed SF was dissolved at a concentration of 20% w/V in 9.3 M aqueous LiBr at 65 °C for 4 h. To eliminate LiBr, the solution was dialyzed in a Slide-A-Lyzer Dialysis Cassette with 3.5 kDa MWCO (Thermo Fisher Scientific, Waltham, MA, U.S.A.), against DI water for 3 days, with regular water changes. Finally, SF aqueous solution was filtered to eliminate any solid residue in suspension and the concentration was measured and adjusted to 8% w/V.

Preparation of Scaffolds. Porous SF scaffolds were produced by solvent casting and particulate leaching method, as described by Rockwood et al.[19] Briefly, 14 g of granular NaCl (particle size between 425 and 800 μm) were added in a polystyrene Petri dish, and 6.5 mL of 8% w/V fibroin aqueous solution were poured on the salt (NaCl (g) to fibroin (g) was 25 to 1). After 48 h at room temperature, gelation of SF solution occurred. NaCl was then removed by washing samples in DI water for 4 days, with regular water changes. Cylindrical-shaped scaffolds of 3 mm in thickness, 6 mm in diameter, and 6 mg in weight were obtained using a 6 mm biopsy punch; afterward, samples were frozen and freeze-dried to remove water. GYY4137 was dissolved in DMSO to prepare three solutions at different concentration (1.5, 7.5, and 15.0 mg/mL of GYY4137 in DMSO, respectively). Each scaffold was impregnated with 40 μL of GYY4137 solution in DMSO, and GYY4137-loaded scaffolds with 1%, 5% and 10% content of GYY4137 in weight with respect to the SF weight were prepared. A set of samples where only pure anhydrous DMSO was poured on the scaffolds was also prepared. The scaffolds were then frozen at −80 °C, and freeze-dried to remove DMSO. The volume of loading solution was chosen on the basis of DMSO uptake by the scaffolds which was determined as equal to 6.9 ± 1.0 times the weight of each scaffold.

All scaffolds were sterilized by Cobalt-60 gamma (γ) irradiation in a standard cycle of 25.0 kGy (nominal dose) by Sterigenics Italy (Minerbio, Italy). Facilities and control procedures validated in conformity with the guidelines ISO 9001, ISO 13485, EN ISO 13485, and good manufacturing practices (GMP) were used.

The different types of scaffolds obtained starting from fibroin solution and the sample codes are listed in Figure 2.

Sample Characterization. *Scanning Electron Microscopy.* For the morphological characterization, SF scaffolds were sputter-coated with a thin platinum/palladium layer (by a Q150T Turbo-Pumped Sputter Coater/Carbon Coater, Quorum Technologies, U.K.), and then observed with a Field Emission Scanning Electron Microscope (FE-SEM, Zeiss Supra 40, Carl Zeiss, Germany), in secondary electron mode. Pore size was calculated with Image-J software (NIH,

DOI: 10.1021/acsbiomaterials.8b00212
ACS Biomater. Sci. Eng. XXXX, XXX, XXX−XXX

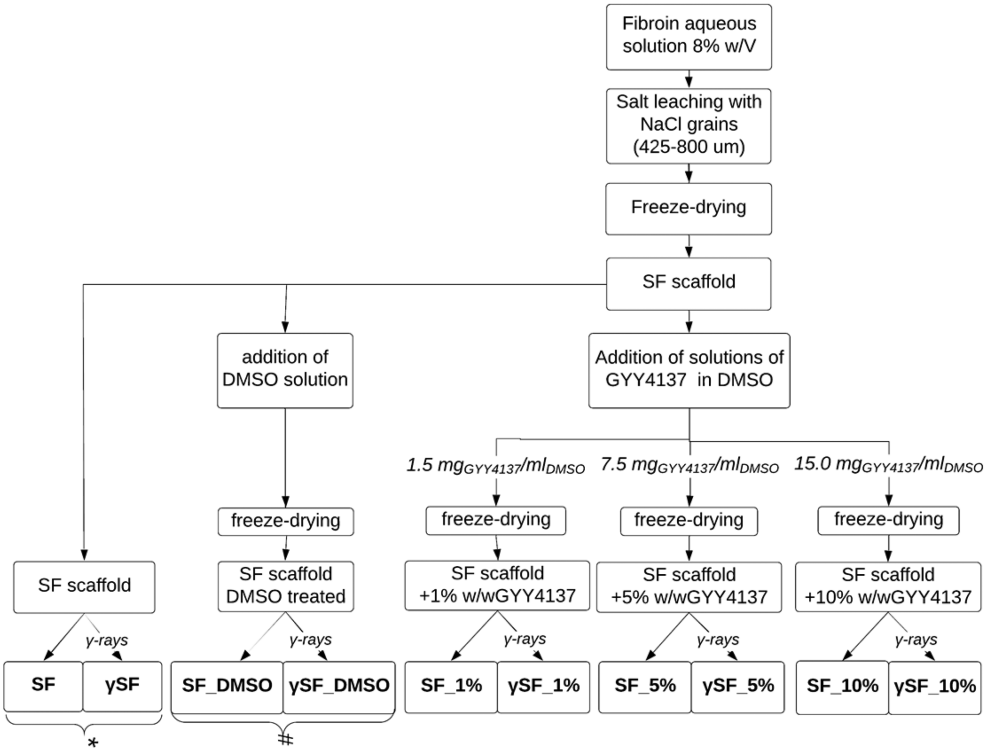

Figure 2. Scheme of the preparation procedure, composition and codes of the scaffolds fabricated. In parallel with GYY4137-loaded scaffolds, also scaffolds treated with DMSO (#) and untreated fibroin scaffolds (*) were produced as controls.

U.S.A.), measuring around 100 pores for each group. Pore size distribution was evaluated using OriginPro 8 (OriginLab, U.S.A.) software, and expressed as mean ± standard error of the mean (SEM). Gaussian distribution of pores was assumed.

Fourier Transform Infrared (FT-IR) Spectroscopy. Fourier transform infrared spectroscopy was used to investigate the chemico-physical properties of the materials fabricated. A Spectrum One FT-IR spectrometer (PerkinElmer, Waltham, MA, U.S.A.) working in attenuated total internal reflection (ATR) mode was used to collect the spectra of the different materials. Four scans for each spectrum were registered in the wavenumber range 4000−650 cm^{-1}, with a resolution of 4 cm^{-1}. FTIR spectra peaks were detected by SEARCH Plus Software for PerkinElmer Spectrum One FTIR (PerkinElmer, Waltham, MA, U.S.A.), and assigned to specific vibrations.[34]

To study the influence of the preparation of GYY4137-loaded scaffolds on GYY4137 chemical properties, commercial GYY4137 was solubilized in DMSO at 15 mg/mL, lyophilized and characterized by FT-IR before and after treatment with γ-irradiation. The samples considered are listed in Table 1.

Table 1. Different Forms of GYY4137 Considered in This Work

material code	details
GYY	commercial GYY4137
γGYY	commercial GYY4137, γ-irradiated
GYY_exDMSO	GYY4137 solubilized in DMSO, freeze-dried
γGYY_exDMSO	GYY4137 solubilized in DMSO, freeze-dried, γ-irradiated

GYY4137-loaded scaffolds were analyzed by FT-IR to assess the presence of GYY4137 in the SF matrices, and to determine SF conformation. In particular, SF secondary structures in the scaffolds were determined by analyzing the Amide I region (1705−1610 cm^{-1}) of the correspondent FTIR spectra, by OriginPro 8 (OriginLab, U.S.A.). Amide I regions were selected and smoothed with a nine-point Savitzky-Golay smoothing filter. Then, Fourier self-deconvolution (FDS tool of OriginPro 8) was applied, using the wavenumber ranges adapted from literature of seven fitting peaks.[35,36] The seven peaks, assumed to be Gaussian, were assigned to the four different proteins secondary structures considered for SF (β-sheet, random coil, α-helix and turns), as reported in Table 2.

Table 2. Vibrational Band Assignments for the Amide I IR Region of Fibroin Spectra Adapted from Ref 35

wavenumber range (cm^{-1})	band assignment
1616−1621	β-sheet
1622−1637	β-sheet
1638−1655	random coil
1656−1662	α-helix
1663−1670	turns
1671−1696	turns
1697−1703	β-sheet

The content percentage of secondary structures present in the scaffolds was calculated by integrating the area of each deconvoluted peak and then normalizing to the total area of the Amide I spectra region analyzed.

Solid-State Nuclear Magnetic Resonance (NMR) Spectroscopy. NMR analyses were performed on ^{13}C and ^{31}P nuclei. The study of ^{13}C nuclei was used for the characterization of GYY4137, before and after solubilization in DMSO and treatment with γ-irradiation, and of GYY4137-loaded scaffolds. In particular, since ^{13}C chemical shift is an intrinsic and sensitive parameter for the evaluation of protein conformations, it was used to examine the possible conformational behavior of SF induced by the scaffold preparation processes. Following a profile fitting of SF alanine $^{13}C\beta$ peak previously reported, the dominant polymorphic conformation between Silk II (β-sheets crystals in amorphous matrix) and Silk I (random coil, turn and α-helix structures) adopted by the protein in the scaffolds was calculated.[37,38] Since GYY4137 molecules contain a phosphorus atom, ^{31}P NMR was used for the selective study of GYY4137 chemical shifts.

DOI: 10.1021/acsbiomaterials.8b00212
ACS Biomater. Sci. Eng. XXXX, XXX, XXX−XXX

NMR analyses were performed with a Bruker 400WB spectrometer (Bruker Corporation, Billerica, MA, U.S.A.) operating at a proton frequency of 400.13 MHz. NMR spectra were acquired with cross-polarization (CP) and single pulse (SP) sequences, under the following conditions: for ^{13}C, frequency 100.23 MHz, $\pi/2$ 3.4 μs, contact time 2 ms, decoupling length 6.7 μs, recycle delay 5 and 30 s for CP and SP respectively, 2k scans; for ^{31}P, frequency 162.49 MHz, $\pi/2$ 3.65 μs, contact time 5 ms, decoupling length 6.7 μs, recycle delay 5 and 100 s for for CP and SP respectively, 8 scans (1k scans for loaded sponges). Samples were packed in 4 mm zirconia rotors, which were spun at 7.5 kHz under air flow. Adamantane CH2 at 38.5 ppm and ammonium dihydrogen phosphate at 0.81 ppm were used as external secondary references for ^{13}C and ^{31}P, respectively.

Differential Scanning Calorimetry (DSC) and Thermogravimetric Analysis (TGA). DSC and TGA techniques were used to investigate the thermal behavior of GYY4137 and the GYY4137-loaded scaffolds. DSC experiments were performed using a DSC20 calorimeter (Mettler-Toledo, Milan, Italy). For each sample, approximately 15 mg of material were placed in aluminum pans and tested under flushing nitrogen (100 mL/min), in the temperature range 30−330 °C, at a heating rate of 10 °C/min. TGA was conducted in a TA Instruments Q5000 thermobalance, testing about 10 mg of material in freshly cleaned platinum pans, under N_2 flow (10 mL/min), in the temperature range 30−700 °C, at a heating rate of 10 °C/min.

Water Uptake Measurement. To measure the water uptake of the scaffolds, the samples were immersed in DI water and placed at 37 °C. Then, an excess of water was removed from the sample surfaces by gently dabbing with paper and the wet weight (W_{wet}) was determined. The same procedure was repeated at various time intervals until W_{wet} was stable. Samples were then dried in oven at 65 °C overnight and the dry weight (W_{dry}) was determined. The water uptake was calculated as $(W_{wet} - W_{dry})/W_{dry}$. Values were expressed as mean with SEM (n = 3 samples for each group).

Amperometric Detection of H_2S Release. H_2S release was measured during incubation of the scaffolds in aqueous PBS 0.01 M at pH 7.4, at room temperature, in the presence of L-cysteine 4 mM. Three replicates of each sample were studied. The concentration of hydrogen sulfide in the incubation medium was monitored for 2.5 h, with a sulfide gas amperometric microsensor H_2S-500 (Unisense, Aarhus N, Denmark), connected to a microsensor multimeter (Unisense, Aarhus N, Denmark) as amplifier for data acquisition. The signal was collected in mV, and converted in concentration units. The H_2S microsensor was calibrated with Na_2S*9H_2O 0.01 M dissolved in a N_2-flushed solution buffered at pH 3.6, in accordance with manufacturer instructions.[39]

Cell Culture. NIH/3T3 embryonic mouse fibroblasts and hMSCs were used for in vitro studies conducted on fibroin scaffolds with different contents of GYY4137. NIH/3T3 cells (Istituto Zooprofilattico Sperimentale della Lombardia e dell'Emilia Romagna, Italy) were cultured in Dulbecco's Modified Eagle's Medium (DMEM) (EuroClone, Pero, Italy) supplemented with 10% fetal bovine serum (FBS), 1% of Antibiotic-Antimycotic 100×, 2 mM L-Glutamine 100×, and 1 mM Sodium Pyruvate 100×. hMSCs (Istituto Ortopedico Rizzoli, Bologna, Italy) were obtained as previously described.[8,40] hMSCs were isolated from bone marrow aspirate during hip-replacement surgery of 2 posttraumatic patients. The cells were washed twice and suspended in α-MEM with 15% FBS (Lonza, Basel, Switzerland), counted, and plated in flask. After 1 week, the nonadherent cells were removed, and the adherent hMSCs were expanded in vitro. hMSCs were used at passage 3 in culture. Cells of both lines were subcultured as monolayers at 37 °C, in 5% CO_2 atmosphere, and medium was changed every 2−3 days. Cells were detached when they reached 80% confluence, according to standard protocols, and used for the experiments. In particular, cells were counted and suspended in culture medium. Then, sterile fibroin scaffolds of all the different compositions were placed in 96-well plates and preconditioned for 10 min with culture medium that was removed before cell seeding. A volume of 50 μL of cell suspension containing 5×10^3 cells was deposited on the top of each cylindrical scaffold (3 mm in thickness, 6 mm in diameter and 6 mg in weight), and 96-well plates were incubated at 37 °C, in 5% CO_2 atmosphere, for 1 h ("drop confined" cell seeding method). Finally, more culture medium was added to each well containing the scaffolds in order to obtain a total volume of 200 μL of medium/well, which could submerge the scaffolds. Seeded cells were maintained at 37 °C, in 5% CO_2 atmosphere for 24 h.

Measurement of In Vitro Cytotoxicity of GYY4137-Loaded Scaffolds. Lactate dehydrogenase (LDH) enzyme released into the medium from cells cultured in the presence of the scaffolds was measured, and used as a biomarker for the evaluation of cellular toxicity and lysis. The potential cytotoxicity effect was measured for silk fibroin scaffolds loaded with different concentrations of GYY4137, untreated fibroin scaffolds, and scaffolds treated with DMSO; the values were then compared with positive and negative controls, respectively, cells seeded on plastic then lysed, and healthy cells seeded on plastic, at a density of 5×10^3 cells/well.

Cells seeded on scaffolds and control wells in the conditions previously described were cultured for 24 h, and then positive control for the LDH assay was prepared by inducing lysis with Triton X-100 surfactant in cells cultured on tissue culture plate. After cell lysis in positive control wells occurred (in around 1 h), all media from positive and negative controls, and from scaffold-containing wells were collected, centrifuged to remove cell debris, and transferred into a new plate to be tested. Lactic dehydrogenase-based assay (TOX7, Sigma-Aldrich) was performed according to manufacturer's instructions. Absorbance was measured using a microplate reader (Spark 10M, Tecan Group, Männedorf, Switzerland) at 490 nm, with background absorbance measured at 690 nm. Results were presented as mean with SEM (n = 5 and n = 2, for experiments with 3T3 and hMSC cells respectively). Statistical analysis was conducted by one-way analysis of variance (ANOVA) using GraphPad Prism version 5.03 (GraphPad software, CA, U.S.A.), and Bonferroni's multiple comparison test was used to evaluate significant differences among the cytotoxicity induced by the different groups of scaffolds. Two sets of samples were considered significantly different when $p < 0.05$.

RESULTS

As previously described, SF porous scaffolds were prepared by processing SF solutions with solvent casting and particulate leaching method, using granular NaCl with particle size between 425 and 800 μm. The scaffolds were either left untreated or loaded with different amounts of GYY4137 by using DMSO as vehicle. Finally, freeze-dried scaffolds were γ-irradiated to obtain sterile products. All sample characterizations were performed before and after the sterilization procedure by γ-irradiation, which did not induce any changes in the properties of the scaffolds. Thus, only the results collected for γ-irradiated samples were reported and discussed in this work.

Microstructure and Porosity of Scaffolds. The morphology of the SF scaffolds, untreated and loaded with different amounts of GYY4137, was investigated by scanning electron microscopy. SEM images of Figure 3A revealed similar morphology characteristics for all the groups of scaffolds prepared. The scaffolds showed a highly porous sponge-like structure. The round-shaped pores appeared homogeneously distributed and characterized by a high degree of interconnectivity. A bimodal distribution of the pore dimensions could be appreciated (Figure 3B). The larger pores had an average size of 350 ± 8 μm, 365 ± 8 μm, 369 ± 5 μm, and 378 ± 4 μm, for γSF, γSF_1%, γSF_5%, and γSF_10%, respectively. The smaller pores, distributed on the surfaces of the large pores and creating an interconnected network between them, had an average size of 61 ± 4 μm, 73 ± 5 μm, 90 ± 5 μm, and 95 ± 7 μm, for γSF, γSF_1%, γSF_5%, and γSF_10% respectively. Even at high values of magnification, neither

DOI: 10.1021/acsbiomaterials.8b00212
ACS Biomater. Sci. Eng. XXXX, XXX, XXX−XXX

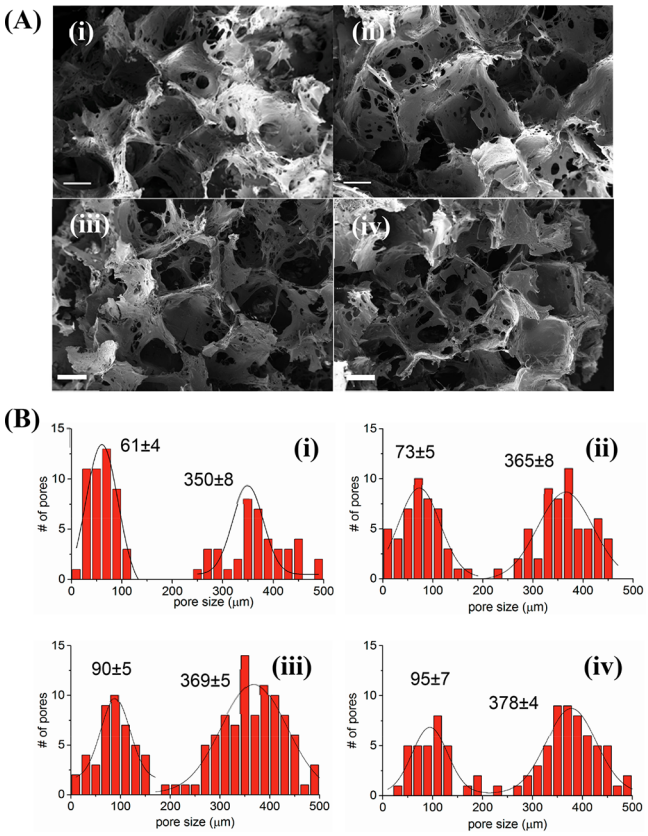

Figure 3. (A) FESEM images of the internal porous structure of dry γ-irradiated SF scaffolds: (i) γSF, untreated scaffold; (ii) γSF_1%, scaffold containing 1%GYY4137; (iii) γSF_5%, scaffold containing 5% GYY4137; (iv) γSF_10%, scaffold containing 10%GYY4137; scale bar 200 μm. (B) Pore size bimodal distributions measured from FESEM images of samples: (i) γSF; (ii) γSF_1%; (iii) γSF_5%; (iv) γSF_10%, with mean ± standard error expressed in micrometers calculated for each distribution.

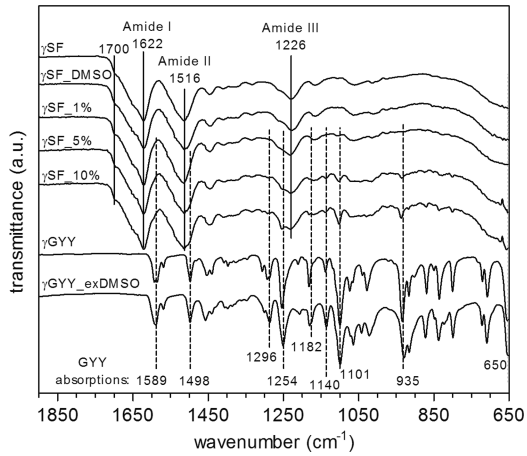

Figure 4. Comparison between the IR spectra of γGYY (γ-irradiated GYY4137 reagent) and γGYY_exDMSO (GYY4137 solubilized in DMSO and lyophilized), and IR spectra of γ-irradiated fibroin scaffolds: γSF, untreated; γSF_DMSO, treated with DMSO; γSF_1%, containing 1% of GYY4137; γSF_5%, containing 5% of GYY4137; γSF_10%, containing 10% of GYY4137. Solid lines indicate absorption bands characteristic of SF; dashed lines indicate peaks of GYY4137 discussed in the text.

crystals nor agglomerates of GYY4137 were visible on GYY4137-loaded fibroin matrices (images not shown).

FT-IR Spectroscopy. Infrared spectroscopy was used to investigate the chemical structure of GYY4137 and GYY4137_exDMSO, and the composition of GYY4137-loaded scaffolds. In addition, FTIR bands of SF were used to study the protein secondary structure in the scaffolds.

Figure 4 showed that γGYY and γGYY_exDMSO had similar spectrum profiles. Moreover, their absorption bands were consistent with the infrared spectrum of GYY4137 previously reported in Alexander et al.[10] The assignments of the bands of samples γGYY and γGYY_exDMSO to specific groups vibrations are proposed in Table 3.

The band assigned to P—S bond stretch, visible at 650 cm^{-1}, was maintained on both spectra.[16] However, some changes in peak relative intensities and shape before and after dissolution of GYY4137 in DMSO and lyophilization were clearly visible, especially for peaks at 1593 cm^{-1}, 1453 cm^{-1}, 1182 cm^{-1}, around 1028 cm^{-1}, and 935 cm^{-1}. Most of these absorption peaks can be assigned to vibrations of C−N and C−O bonds present in the structure of the two morpholine groups of GYY4137 molecule.

Figure 4 also reported the FTIR spectra of GYY4137-loaded scaffolds and, for comparison, the spectra of γSF and γSF_DMSO. Curves of γSF and γSF_DMSO were both characterized by the typical protein backbone absorption bands, i.e. Amide I, II, and III, which are very useful for conformation studies.[41,42] In particular, Amide I and Amide II bands appeared broad and centered at wavenumbers correlated with a prevalence of β-sheet secondary structure, respectively, at 1622 and 1516 cm^{-1}.[35,38] Amide I presented a shoulder at 1690 cm^{-1}, suggesting the presence of β-sheet crystallinity of the antiparallel type.[43] Amide III band was centered at 1226 cm^{-1}, with a shoulder at 1265 cm^{-1}, confirming that β-sheet was the main conformation adopted by fibroin in γSF scaffold.

Curves of GYY4137-loaded fibroin scaffolds (i.e., γSF_1%, γSF_5%, and γSF_10%) exhibited absorption profiles similar to samples γSF and γSF_DMSO for Amide I, II, and III bands. In addition, peaks derived from the presence of GYY4137 were clearly visible only for samples γSF_5% and γSF_10% and their intensity increased proportionally with the amount of GYY4137 incorporated in the scaffolds. The curve of γSF_5% presented peaks at 1593 and 1498 cm^{-1}, 1296 cm^{-1}, 1254 cm^{-1}, 1182 cm^{-1}, 1140 cm^{-1}, 1101 cm^{-1}, 935 cm^{-1}, and between 835 and 800 cm^{-1}, related to GYY4137 absorptions. γSF_10% spectrum featured similar but more intense absorption frequencies deriving from the presence of GYY4137. However, it was not possible to appreciate if these absorptions were more similar to those detected for γGYY or for γGYY_exDMSO.

The results of the protein Amide I analysis are reported in Figure 5A and showed similar amounts of secondary structures for all the scaffolds. In particular, the scaffolds displayed similar amounts of β-sheet. Fibroin had 53%, 53%, 56%, 55% and 54% of β-sheet secondary structure respectively in γSF, γSF_DMSO, γSF_1%, γSF_5% and γSF_10%. The differences between these values were considered not significant. The rest of the protein was mainly organized in random coil and turn structures, with a small amount of α-helix. Figure 5B shows an example of an absorbance spectrum of Amide I, deduced after Fourier self-deconvolution with seven peaks, as described previously in this manuscript. The different secondary

DOI: 10.1021/acsbiomaterials.8b00212
ACS Biomater. Sci. Eng. XXXX, XXX, XXX−XXX

Table 3. Infrared Vibrational Bands and Assignments of Samples γGYY and γGYY_exDMSO (GYY4137 Solubilized and Lyophilized in DMSO)

γGYY ν (cm^{-1})	γGYY_exDMSO ν (cm^{-1})	band assignment
1593, 1586, 1569, 1498	1589, 1569, 1498	aromatic C═C stretch (1600−1475) and N−H bend above 1550
1453, 1440	1457	alkanes C−H deformation
1408, 1397	1398	CH_3 bend
1306, 1293	1286	C−N vibrations
1254	1251	aromatic C−O stretch (pheyl-O-alkyl)
1181, 1138	1180, 1136	C−N vibrations and C−O−C stretch
1099	1099	C−O and/or C−N stretch
1073, 1040	1064, 1042	n.a.
1028	1022	phenyl-O-alkyl
934, 916, 902	929, 915	n.a.
869	872	para substituted aromatic ring C−H deformation
836	837	benzene ring C−H deformation
800	799	=C−H aromatics or N−H (out-of-plane bend)
721, 708	722, 709	benzene ring C−H deformation
650	650	P═S stretch

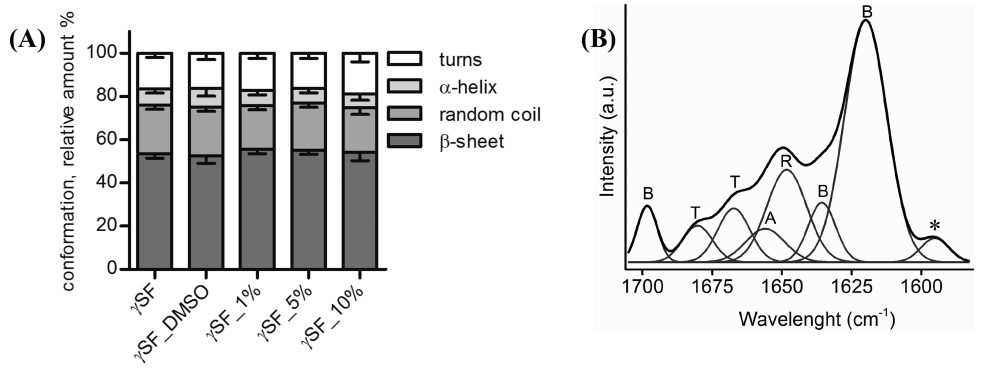

Figure 5. (A) Percentages of the main four different secondary structure (β-sheet, random coil, α-helix, turns) contributing to fibroin Amide I band. Samples are γSF, untreated scaffold; γSF_1%, scaffold containing 1% of GYY4137; γSF_5%, scaffold containing 5% of GYY4137; γSF_10%, scaffold containing 10% of GYY4137. Mean with SD, n = 3. (B) Example of an absorbance spectrum of Amide I, deduced after Fourier self-deconvolution with seven peaks. B is β-sheet, T is turns, A is α-helix and R is random coil. Peak marked with * is assigned to tyrosine side chains, not considered in the quantification of the secondary structure.

structure contributions are highlighted with B for β-sheet, T for turns, A for α-helix, and R for random coil.

NMR Analysis. The ^{13}C CPMAS NMR spectra of relevant samples are shown in Figure 6.

Sharp signals and two broad peaks characterized the spectrum profile of γGYY (assignments based on GYY4137 labeled structure in Figure 6 and reported in Table 4). After dissolution of GYY4137 in DMSO and lyophilization, in the ^{13}C spectrum the sharpness of the peaks increased, suggesting improved crystallinity. However, the peaks did not show any shift in position, thus confirming that the dissolution in DMSO did not substantially alter the molecular structure.

The ^{13}C CPMAS NMR spectra of samples γSF and γSF_10% were both dominated by the signals belonging to the amino acid main sequence AGS(Y)GAG in SF.[38,44] Unfortunately, the intense SF resonances hindered the possibility of observing the weak GYY4137 peaks in the spectrum of 10% GYY4137-loaded scaffold. Only the small peak at 163 ppm, which was attributed to C12, was a proof of the presence of adsorbed GYY4137. Comparing the fibroin signals in the two samples, small differences could be appreciated in the case of Ala/Gly C═O peak centered at 172 ppm, and Ala CH_3 signal (Cβ) centered at 18 ppm. Moreover, the appearance of a high-field shoulder on the Gly CH_2 resonance (Cα) at 42 ppm could be observed. According to previous reports that pointed out the high sensitivity of SF secondary structure to processing treatments, the profile fitting procedure was applied to the Ala Cβ peak of γSF, γSF_DMSO and γSF_10% spectra, in order to evaluate the percentage of the possible SF conformations.[38] The fibroin sponge used in the present work presented 61% of Silk II conformation, which increased up to 65% in γSF_DMSO and reached 74% in the γSF_10%.

In order to better characterize the features of GYY4137 in the different samples, the ^{31}P CPMAS NMR spectra were recorded (Figure 7). Since fibroin does not contain any phosphorus atoms, it was possible to selectively characterize the H_2S donor inside the loaded scaffolds, and compare the results with the characterization conducted on γGYY.

The ^{31}P CPMAS NMR spectrum of γGYY was characterized by a single sharp peak at 90.5 ppm. The recrystallization after DMSO (γGYY_exDMSO) produced a moderately asymmetric and enlarged resonance at the same position. The spectrum of sample γSF_1% is not shown, since the peak is beyond the sensitivity limits. The adsorption of 5 and 10% GYY4137 on SF scaffolds (γSF_5% and γSF_10%) did not affect the H_2S donor structure and the peak intensity was in agreement with the different nominal GYY4137 loadings.

DOI: 10.1021/acsbiomaterials.8b00212
ACS Biomater. Sci. Eng. XXXX, XXX, XXX−XXX

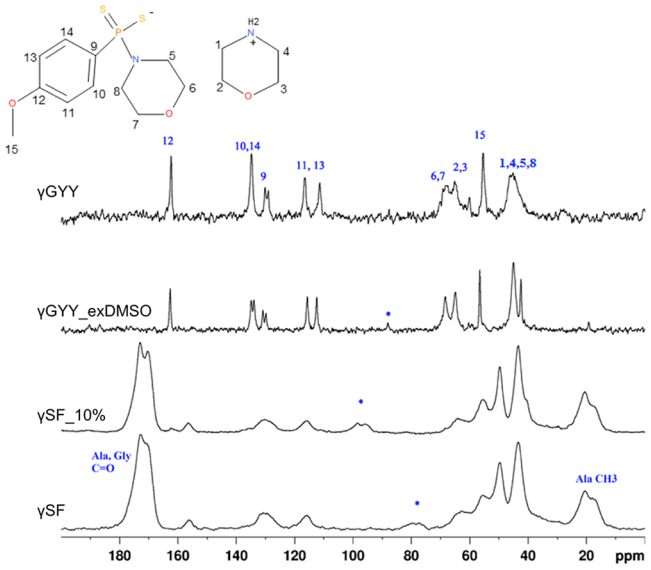

Figure 6. ^{13}C CPMAS NMR spectra of γSF (untreated scaffold), γSF_10% (containing 10% of GYY4137), γGYY (γ-irradiated GYY4137 reagent), γGYY_exDMSO (GYY4137 solubilized and lyophilized in DMSO), and GYY4137 molecular structure with C atoms numbering scheme. Spinning sidebands are marked with *.

Table 4. ^{13}C NMR Chemical Shifts of γGYY and Assignments[10]

	γGYY	
δ (ppm)	functional group	C labeling
45.2	$N(CH_2)_2$ morpholinium	1, 4
45.2	$N(CH_2)_2$ morpholinium attached to P	5, 8
55.5	OCH_3	15
65.0	$O(CH_2)_2$ morpholinium	2, 3
68.3	$O(CH_2)_2$ morpholinium attached to P	6, 7
111.4/116.6	arylCH *o*- to OMe	11, 13
129.2/130.2	arylC-P	9
134.9	arylCH *o*- to P	10, 14
162.7	arylC-OMe	12

Thermal Analyses: DSC and TGA. The thermal behavior of GYY4137 and GYY4137-loaded scaffolds was studied by DSC and TGA. Figure 8A reports DSC thermogram of γGYY powders, showing two endothermic peaks, centered at T^I = 123 °C (Δ*H* = 54 J/g), and T^{II} = 169 °C (Δ*H* = 63 J/g), related respectively to the decomposition of morpholinium and the melting of (*p*-methoxyphenyl)morpholino-phosphinodithioate.[10,11]

Figure 8B showed the thermograms of GYY4137-loaded scaffolds compared to γSF. All the scaffolds were characterized by a wide endothermic peak centered around 95 °C (T_e), related to the loss of absorbed water, and a sharp endothermic peak centered at higher temperatures, around 288 °C (T_d), due to the thermal degradation of the protein.[38,45−47] In particular, degradation of γSF scaffold occurred approximately at 293 °C (Δ*H* = 168 J/g), with a sharp endothermic peak. GYY4137-loaded scaffolds showed wider degradation peaks with a shift over lower temperatures and lower values of the associated enthalpy. These differences became more evident increasing the amount of loaded GYY4137 from sample γSF_1% (T_d = 290 °C, Δ*H* = 150 J/g), to γSF_5% (T_d = 289 °C, Δ*H* = 127 J/g) and γSF_10% (T_d = 283 °C, Δ*H* = 136 J/g).

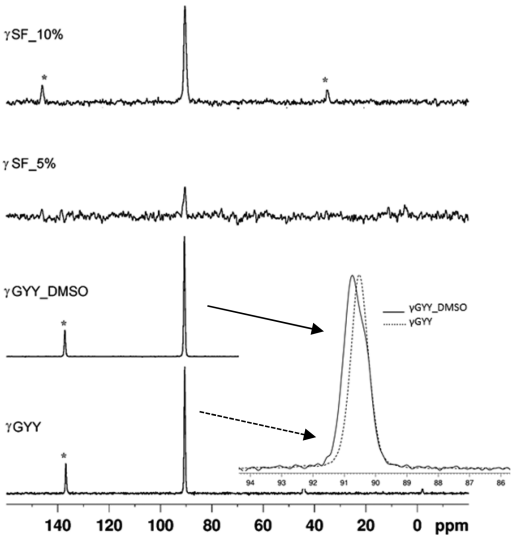

Figure 7. ^{31}P CPMAS NMR spectra of γGYY (γ-irradiated GYY4137 reagent), γGYY_exDMSO (GYY4137 solubilized and lyophilized in DMSO), γSF_5% (containing 5% of GYY4137), γSF_10% (containing 10% of GYY4137). Spinning sidebands are marked with *. The inset shows the profiles of the ^{31}P peaks at 90.5 ppm of γGYY and γGYY_exDMSO.

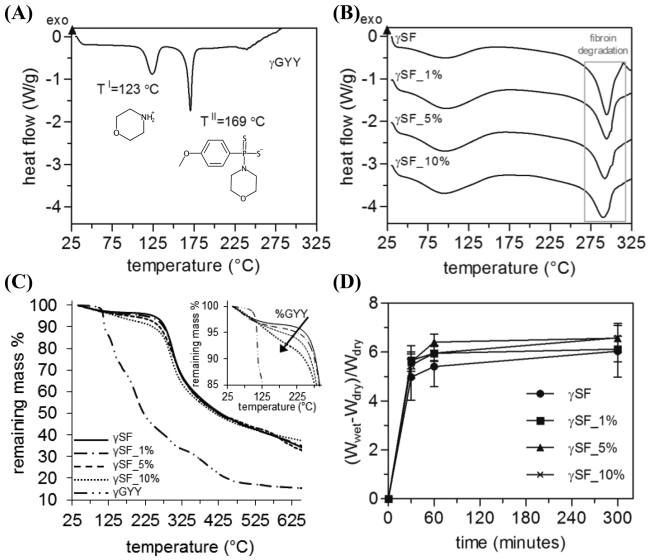

Figure 8. DSC curve obtained for (A) γ-irradiated GYY4137 and for (B) γ-irradiated SF scaffolds. (C) TGA analyses of the different SF scaffolds and of γGYY; the inset highlights mass losses in the scaffolds in the temperature range of GYY4137 degradation. GYY4137 content increases in the direction of the arrow. (D) Water uptake curves of the scaffolds incubated in water at 37 °C (mean with SEM, *n* = 3). Samples are γSF, untreated fibroin scaffold; γSF_1%, scaffold with 1% of GYY4137; γSF_5%, scaffold with 5% of GYY4137; γSF_10%, scaffold with 10% of GYY4137; γGYY, γ-irradiated GYY4137 reagent.

Interestingly, thermal transitions related to GYY4137 were not visible on the thermograms of scaffolds γSF_1%, γSF_5%, and γSF_10%.

TGA gave the mass losses occurred in γGYY powders and in GYY4137-loaded scaffolds during heating from room temperature up to 700 °C. As shown in Figure 8C, the most relevant mass loss in γGYY powders (around 60% of the initial weight

DOI: 10.1021/acsbiomaterials.8b00212
ACS Biomater. Sci. Eng. XXXX, XXX, XXX−XXX

of the sample) occurred between 150 and 300 °C. In the same temperature range, a visible mass loss could be monitored for scaffolds loaded with GYY4137, but not for γSF: the mass loss % resulted proportional to the amount of GYY4137 loaded into the SF sponges. Above 300 °C (i.e., after the beginning of fibroin degradation), most of the weight was lost from all the scaffolds, leaving a residue of around 30% at 700 °C.

Water Uptake Evaluation. The curves of the water uptake of the scaffolds were reported in Figure 8D and showed comparable profiles for the different samples. The process of water uptaking was completed after 60 min of incubation. After 300 min, the weight of wet scaffolds was stable and was used to calculate the water uptake as $(W_{wet} - W_{dry})/W_{dry}$. Water uptake measured 6.0 ± 1.8 for scaffold γSF, 7.8 ± 2.0 for γSF_1%, 6.1 ± 0.9 for γSF_5%, and 6.6 ± 1.0 for γSF_10%.

Release of H_2S from GYY4137-Loaded Scaffolds. Amperometry was used for the continuous record of H_2S in the incubation media of GYY4137-loaded scaffolds. The H_2S-microsensor measured the concentration of the undissociated species indicated as H_2S in the equilibrium: $H_2S \rightleftarrows HS^- \rightleftarrows S^{2-}$, with $pK_{a1} = 6.9$ and $pK_{a2} > 11$. It can be calculated that, at pH 7.4, the concentration of H_2S is approximately 30% of the total dissolved sulfide (i.e., $H_2S + HS^- + S^{2-}$).[48−50]

Measurements of the concentration of H_2S were collected in continuum for 2.5 h in the incubation media of GYY4137-loaded scaffolds and compared with the results obtained for γSF and γSF_DMSO, which did not release H_2S. Figure 9A showed the curves of H_2S generation in solution during time. All the GYY4137-loaded fibroin sponges induced a sustained release of H_2S, but the concentration levels reached at plateau gradually increased with the GYY4137 content of the scaffolds. γSF_1% generated a maximum concentration of 6.5 μM of H_2S during the 2.5 h of the experiment. H_2S concentration profile for γSF_5% was similar, but reached higher values at the plateau, settling at 9 μM. Finally, γSF_10% generated the highest concentration of H_2S in solution: the H_2S curve increased over the first 100 min of incubation and then reached plateau at a concentration of around 31 μM.

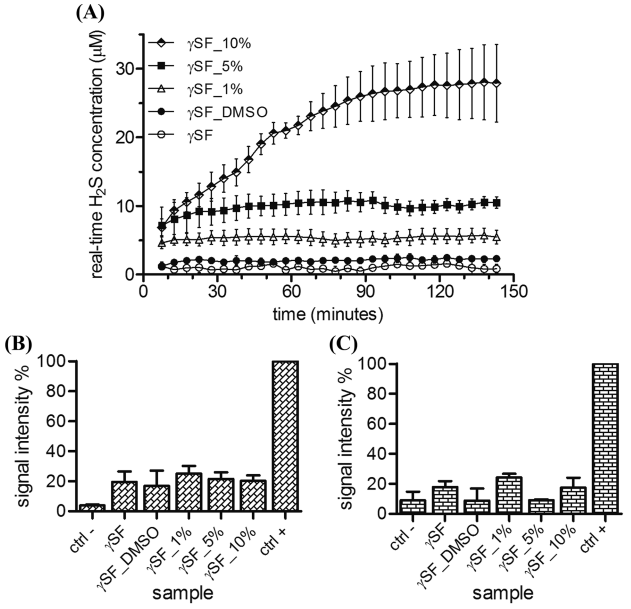

Figure 9. (A) Release of H_2S monitored by H_2S-selective microelectrode for SF scaffolds incubated in PBS pH 7.4 with L-cysteine 4 mM, at room temperature (mean with SEM, $n = 4$); error bars are not visible when lying within dimensions of symbols. Cytotoxicity of the different groups of scaffolds (γSF_DMSO, treated with DMSO; γSF_1%, containing 1% of GYY4137; γSF_5%, containing 5% of GYY4137; γSF_10%, containing 10% of GYY4137) on (B) 3T3 cells and on (C) hMSCs, expressed as signal intensity %, proportional to LDH released in the supernatants, respect to ctrl+. Cells cultured on plastic were used as negative control, while cells treated with 0.05% Triton X-100 surfactant were used as positive control (100% of LDH release). The values are expressed as mean with SEM ($n = 5$ for 3T3 and $n = 2$ for hMSC).

In Vitro Experiments: Cytotoxicity of GYY4137-Loaded Scaffolds. In two parallel experiments, 3T3 murine fibroblasts and hMSCs were cultured in the presence of the scaffolds of all the different compositions, for 24 h. The amount of LDH released in culture media from the cells was measured and used to determine the potential toxic effects of the scaffolds, by comparison with the results obtained for positive and negative control samples. The results of the LDH assays are shown in Figure 9B,C. For both cell types, the mean value of % of cytotoxicity calculated for γSF scaffolds was around 19%, confirming that salt-leached fibroin matrices ensured the viability of seeded cells, as previously demonstrated.[31] Similarly, also the cytotoxicity induced by γSF_DMSO, that is, the scaffold contacted with DMSO but not containing GYY4137, was limited. The amount of LDH released by 3T3 cells did not increase for GYY4137-loaded scaffolds, which induced only between 20% and 25% of cytotoxicity (i.e., very close to γSF). Likewise, GYY4137-loaded scaffolds resulted also minimally cytotoxic for hMSCs, with some variability between samples that showed 24%, 9%, and 17% of released LDH, respectively for γSF_1%, γSF_5%, and γSF_10%.

DISCUSSION

The current study was intended to the preparation of a novel 3D system to achieve localized and sustained release of H_2S for a future application in bone tissue engineering. A SF matrix, already shown to promote bone cells development,[51] was combined with GYY4137, one of the most appreciated donors of H_2S. In fact, GYY4137 is not toxic and is capable of releasing H_2S "slowly", compared with conventional donors (e.g., NaHS), over extended periods of time, both *in vitro* and *in vivo*.[11] When GYY4137 is put in contact with an aqueous environment, the P═S bonds start to decompose by hydrolysis, and H_2S is generated. Thus, in previous experiments, GYY4137 formulations dissolved in aqueous solution needed to be administered fresh, immediately after the preparation. In this context, the GYY4137-loaded SF scaffolds described in this work represent a novel approach for the administration of GYY4137. Anhydrous DMSO was chosen as solvent and vehicle for the loading of GYY4137 into the sponges because DMSO allowed the preparation of solutions where GYY4137 did not decompose, thus preventing early release of H_2S from GYY4137, as proved by spectroscopic analyses. Moreover, after the loading process, it could be completely removed from the scaffolds by freeze-drying.[52] Dissolution in DMSO and removal of the solvent (γGYY_exDMSO), performed on GYY4137 in order to mimic the loading conditions and study their potential effects, induced only slight modifications in GYY4137 crystal structure, with no chemical changes. We hypothesized that GYY4137 crystals, after DMSO, reformed in a new structure

DOI: 10.1021/acsbiomaterials.8b00212
ACS Biomater. Sci. Eng. XXXX, XXX, XXX−XXX

containing the morpholinium cation in a different arrangement, which caused a diversification of the signals related to morpholine energetic transitions. In fact, both on IR and NMR spectra, some absorption bands assigned to morpholine appeared sharper and better resolved after recrystallization from DMSO. On the other hand, all peaks were maintained on infrared spectra of γGYY_exDMSO, and phosphorus signal was in the same position at 90.5 ppm on ^{31}P NMR spectra. Similarly, the incorporation of GYY4137 into SF scaffolds did not affect the H_2S donor chemical structure: the characteristic bands of GYY4137, when visible, were maintained in the same positions on scaffolds infrared curves, and phosphorus peak on ^{31}P NMR spectra only changed intensity, in agreement with the GYY4137% of loading.

The morphology and, particularly, the porosity are fundamental features of a scaffold for bone tissue engineering applications.[28] Porous matrices made of SF were already proposed as scaffolds to culture and grow bone cells *in vitro* and for guiding new bone tissue formation *in vivo*. Pores with suitable dimensions (more than 300 μm) and distribution are needed, because they allow cell migration and proliferation, as well as vascularization.[26] The microstructure of the different SF sponges produced was investigated by FE-SEM imaging, and we could assess that the loading process with the H_2S donor preserved the original morphology. The absence of visible GYY4137 agglomerates indicated that a fine dispersion of small GYY4137 crystals was obtained inside the SF scaffolds. A highly interconnected porosity with randomly distributed pores was present in all the scaffolds, with no substantial differences between γSF and differently loaded sponges. Salt leaching process left a porosity with large and small pores, with dimensions (up to 500 μm) indicated as appropriate for the formation of bone tissue within the scaffold. Pores were smaller than NaCl grains used because of the partial dissolution of the salt occurred during the addition of the SF solution.

In terms of conformation adopted by fibroin in the scaffolds, infrared spectra showed the positions of the typical protein absorption bands, Amide I, Amide II, and Amide III, which indicated a prevalent β-sheet secondary structure in all the scaffolds, induced by the use of NaCl during the salt leaching process.[53,54] In fact, salt-leached SF scaffolds were stable and did not need any further treatment to be insoluble in water.

The importance to take in account the influence of all the fabrication processing steps on the structure of SF-based materials is well-established.[38] Thus, to investigate possible changes related to the GYY4137-loading process in SF structure and scaffold crystallinity, an analysis of Amide I infrared absorption band was conducted. In particular, the four protein secondary structures considered for fibroin were β-sheet, random coil, α-helix, and turns. The results, shown in Figure 5 for samples γSF, γSF_DMSO, γSF_1%, γSF_5%, and γSF_10%, indicated that all the scaffolds contained comparable relative amount of secondary structure of the β-sheet type. This resulted in the same levels of crystallinity between the SF matrices, thus proving that the highly ordered secondary conformation is stable upon addition of GYY4137.[38,55] The profile fitting conducted on the NMR Cβ Ala peak of SF was used to evaluate the % of Silk II conformation, comprising β-sheet crystals and so-called β-sheet-like structures in an amorphous matrix, in the scaffolds. The result was that manipulation (such as the addition of GYY4137 in γSF_10%) or aging (data not shown) of SF induced a slight increase of the Silk II component. A similar effect for SF materials was already monitored before through the study of the NMR Cβ Ala peak.[56]

DSC analyses indicated that a difference in the SF scaffolds treatment and composition contributed to their thermal behavior during heating. For GYY4137-loaded scaffolds, the degradation peaks were at lower temperatures compared to the γSF. These effects were presumably related to the presence of GYY4137 decomposing before the temperature of SF degradation. We hypothesize that the environment generated locally and diffusely in the SF matrix by the thermal energy exchanges derived from the melting of GYY4137 induced an anticipated degradation of the scaffolds in their entirety. TGA curves, confirmed that evidence: a mass loss could actually be detected in the temperature range 225÷325 °C for γGYY and for the GYY4137-loaded scaffolds, but not for γSF.

The retention of the H_2S releasing abilities of GYY4137 after the loading into the SF scaffolds was a critical point of this work. Since different amounts of GYY4137 were used, we expected to detect quantities of H_2S released in solution upon incubation of the scaffolds proportional to the initial concentrations of GYY4137 w/w% in SF. To assess this point, GYY4137-loaded scaffolds were incubated and H_2S concentration in the media was monitored in continuum, until release curves reached the steady state (i.e., the condition of dynamic equilibrium with constant H_2S concentration monitored in solution). The incubation media contained L-cysteine, as Martelli et al. showed that GYY4137 releases H_2S in a L-cysteine-dependent mechanism, and endogenous organic thiols like this amino acid are always present in biological environments.[13] In previous studies, the kinetic of H_2S generation process was described, and it was assessed that solutions of GYY4137 1 mmol/L in PBS at pH 7.4 generated a peak in H_2S concentration in the first 20 min, which then decreased.[11,13] Moreover, the steady state of H_2S release curves was reported to depend on the combination of different processes: not only the concentration of the H_2S source but also volatilization and oxidation of H_2S dissolved in solution, occurring in parallel at any time.[57] In this work, we could assess that the incorporation of GYY4137 in the SF matrix influenced the process of H_2S generation in solution: the curves of real-time H_2S concentration increased gradually, without evident peaks ascribable to burst release phenomena. Differences between the H_2S release curves related to γSF_1%, γSF_5%, γSF_10% were evidenced: the steady state was reached at higher H_2S concentrations increasing the GYY4137% of loading. The time required to reach the concentration of the plateau was approximately the same for all samples, indicating that the release process occurred at similar rates from all the scaffolds.

The content of GYY4137 in the scaffolds did not have an impact on the viability of the tested cells. To assess this, cells were seeded on the top of the different scaffolds and cultured for 24 h. In this period of time, cells experienced the contact with the upper surface of the scaffolds, and some cells presumably penetrated the scaffolds thanks to the porosity. Moreover, as discussed above on the basis of the curves of real-time H_2S concentration, H_2S formed and diffused in cell culture medium during the incubation. For both 3T3 cells and hMSCs, the progenitors of mature osteoblasts, no significant increase in the cytotoxicity could be detected in cell seeded scaffolds, compared to the negative control. This suggested that the materials tested in the experiment, particularly the different amounts of GYY4137 loaded into the fibroin matrices

DOI: 10.1021/acsbiomaterials.8b00212
ACS Biomater. Sci. Eng. XXXX, XXX, XXX−XXX

and the consequent released H_2S, did not exert any toxic effect on the cell lines, independently from their phenotype.

CONCLUSIONS

In the current study, we provide a proof-of-concept evidence for a novel device based on a long-lasting H_2S release in the tissue microenvironment, targeting applications in tissue engineering of the musculoskeletal system. To pursue this aim, a scaffold-based system suitable for bone was chosen in combination with GYY4137, a donor of H_2S and potential novel modulator of bone cells functions.

A novel process was designed to incorporate the H_2S donor GYY4137 into prefabricated SF porous scaffolds produced by salt leaching method. GYY4137 was incorporated into the scaffolds at different concentrations that were chosen for their capacity to generate specific levels of H_2S in solution upon hydrolysis.[7,8]

In summary, we demonstrated that GYY4137 could be quantitatively incorporated into SF porous matrices, without impairing the original chemico-physical properties of the scaffolds constituents. GYY4137-loaded SF sponges maintained the morphology and protein conformation exhibited by γSF scaffold, and the H_2S-releasing abilities of GYY4137 were preserved. The GYY4137-loaded SF scaffolds dose-dependently released H_2S upon incubation in solution and exhibited no cytotoxic effects, in both mouse fibroblasts and human osteoprogenitor cells.

On the basis of the results obtained, we can assume that SF scaffolds loaded with concentrations of GYY4137 inside the range explored could be suitable for the proposed application. This possibility will be investigated in our future studies.

AUTHOR INFORMATION

Corresponding Authors

*E-mail: antonella.motta@unitn.it.
*E-mail: francesco.grassi@ior.it.

ORCID

Rosasilvia Raggio: 0000-0002-7442-2973

Author Contributions

#(R.R. W.B.) These authors contributed equally to the work.

Notes

The authors declare no competing financial interest.

ACKNOWLEDGMENTS

This study was supported by grant "Ricerca Finalizzata" from the Italian Ministry of Health (RF PE-2011-02348395, title of the project "Novel approach for bone regeneration and repair using sulphur donor-based therapy").

REFERENCES

(1) Li, L.; Rose, P.; Moore, P. K. Hydrogen Sulfide and Cell Signaling. *Annu. Rev. Pharmacol. Toxicol.* **2011**, *51* (1), 169−187.

(2) Vandiver, M. S.; Snyder, S. H. Hydrogen sulfide: A gasotransmitter of clinical relevance. *J. Mol. Med.* **2012**, *90* (3), 255−263.

(3) Abe, K.; Kimura, H. The possible role of hydrogen sulfide as an endogenous neuromodulator. *J. Neurosci.* **1996**, *16* (3), 1066−1071.

(4) Koenitzer, J. R.; Isbell, T. S.; Patel, H. D.; Benavides, G. A.; Dickinson, D. A.; Patel, R. P.; Darley-usmar, V. M.; Lancaster, J. R.; Doeller, J. E.; Kraus, D. W. Hydrogen sulfide mediates vasoactivity in an O_2-dependent manner. *Am J Physiol Heart Circ Physiol.* **2007**, *292*, H1953−H1960.

(5) Fiorucci, S.; Distrutti, E.; Cirino, G.; Wallace, J. L. The Emerging Roles of Hydrogen Sulfide in the Gastrointestinal Tract and Liver. *Gastroenterology* **2006**, *131* (1), 259−271.

(6) Liu, Y.; Yang, R.; Liu, X.; Zhou, Y.; Qu, C.; Kikuiri, T.; Wang, S.; Zandi, E.; Du, J.; Ambudkar, I. S.; et al. Hydrogen sulfide maintains mesenchymal stem cell function and bone homeostasis via regulation of Ca2+ channel sulfhydration. *Cell Stem Cell* **2014**, *15* (1), 66−78.

(7) Gambari, L.; Lisignoli, G.; Cattini, L.; Manferdini, C.; Facchini, A.; Grassi, F. Sodium hydrosulfide inhibits the differentiation of osteoclast progenitor cells via NRF2-dependent mechanism. *Pharmacol. Res.* **2014**, *87*, 99−112.

(8) Grassi, F.; Tyagi, A. M.; Calvert, J. W.; Gambari, L.; Walker, L. D.; Yu, M.; Robinson, J.; Li, J.-Y.; Lisignoli, G.; Vaccaro, C.; et al. Hydrogen Sulfide Is a Novel Regulator of Bone Formation Implicated in the Bone Loss Induced by Estrogen Deficiency. *J. Bone Miner. Res.* **2016**, *31* (5), 949−963.

(9) Calderone, V.; Martelli, A.; Testai, L.; Citi, V.; Breschi, M. C. Using hydrogen sulfide to design and develop drugs. *Expert Opin. Drug Discovery* **2016**, *11* (2), 163−175.

(10) Alexander, B. E.; Coles, S. J.; Fox, B. C.; Khan, T. F.; Maliszewski, J.; Perry, A.; Pitak, M. B.; Whiteman, M.; Wood, M. E. Investigating the generation of hydrogen sulfide from the phosphonamidodithioate slow-release donor GYY4137. *MedChemComm* **2015**, *6* (9), 1649−1655.

(11) Li, L.; Whiteman, M.; Guan, Y. Y.; Neo, K. L.; Cheng, Y.; Lee, S. W.; Zhao, Y.; Baskar, R.; Tan, C.-H.; Moore, P. K. Characterization of a Novel, Water-Soluble Hydrogen Sulfide-Releasing Molecule (GYY4137): New Insights Into the Biology of Hydrogen Sulfide. *Circulation* **2008**, *117* (18), 2351−2360.

(12) Zhao, Y.; Wang, H.; Xian, M. Cysteine-activated hydrogen sulfide (H2S) donors. *J. Am. Chem. Soc.* **2011**, *133* (1), 15−17.

(13) Martelli, A.; Testai, L.; Citi, V.; Marino, A.; Pugliesi, I.; Barresi, E.; Nesi, G.; Rapposelli, S.; Taliani, S.; Da Settimo, F.; et al. Arylthioamides as H2S donors: L-cysteine-activated releasing properties and vascular effects in vitro and in vivo. *ACS Med. Chem. Lett.* **2013**, *4* (10), 904−908.

(14) Li, L.; Salto-Tellez, M.; Tan, C.-H.; Whiteman, M.; Moore, P. K. GYY4137, a novel hydrogen sulfide-releasing molecule, protects against endotoxic shock in the rat. *Free Radical Biol. Med.* **2009**, *47* (1), 103−113.

(15) Liu, Z.; Han, Y.; Li, L.; Lu, H.; Meng, G.; Li, X.; Shirhan, M.; Peh, M. T.; Xie, L.; Zhou, S.; et al. The hydrogen sulfide donor, GYY4137, exhibits anti-atherosclerotic activity in high fat fed apolipoprotein $E^{(-/-)}$ mice. *Br. J. Pharmacol.* **2013**, *169* (8), 1795−1809.

(16) Rose, P.; Dymock, B. W.; Moore, P. K. GYY4137, a novel water-soluble, H2S-releasing molecule. *Methods Enzymol.* **2015**, *554*, 143−167.

(17) Hutmacher, D. W. Scaffolds in tissue engineering bone and cartilage. *Biomaterials* **2000**, *21* (24), 2529−2543.

(18) Vepari, C.; Kaplan, D. L. Silk as a biomaterial. *Prog. Polym. Sci.* **2007**, *32* (8−9), 991−1007.

(19) Rockwood, D. D. N.; Preda, R. R. C.; Yücel, T.; Wang, X.; Lovett, M. L.; Kaplan, D. L. Materials fabrication from Bombyx mori silk fibroin. *Nat. Protoc.* **2011**, *6* (10), 1612−1631.

(20) Melke, J.; Midha, S.; Ghosh, S.; Ito, K.; Hofmann, S. Silk fibroin as biomaterial for bone tissue engineering. *Acta Biomater.* **2016**, *31*, 1−16.

(21) Correia, C.; Bhumiratana, S.; Yan, L.-P.; Oliveira, A. L.; Gimble, J. M.; Rockwood, D.; Kaplan, D. L.; Sousa, R. A.; Reis, R. L.; Vunjak-Novakovic, G. Development of silk-based scaffolds for tissue engineering of bone from human adipose-derived stem cells. *Acta Biomater.* **2012**, *8* (7), 2483−2492.

(22) Nazarov, R.; Jin, H. J.; Kaplan, D. L. Porous 3-D scaffolds from regenerated silk fibroin. *Biomacromolecules* **2004**, *5* (3), 718−726.

(23) Kim, U. J.; Park, J.; Joo Kim, H.; Wada, M.; Kaplan, D. L. Three-dimensional aqueous-derived biomaterial scaffolds from silk fibroin. *Biomaterials* **2005**, *26* (15), 2775−2785.

DOI: 10.1021/acsbiomaterials.8b00212
ACS Biomater. Sci. Eng. XXXX, XXX, XXX−XXX

(24) Yan, L. P.; Oliveira, J. M.; Oliveira, A. L.; Caridade, S. G.; Mano, J. F.; Reis, R. L. Macro/microporous silk fibroin scaffolds with potential for articular cartilage and meniscus tissue engineering applications. *Acta Biomater.* **2012**, *8* (1), 289−301.
(25) Fuchs, S.; Jiang, X.; Schmidt, H.; Dohle, E.; Ghanaati, S.; Orth, C.; Hofmann, A.; Motta, A.; Migliaresi, C.; Kirkpatrick, C. J. Dynamic processes involved in the pre-vascularization of silk fibroin constructs for bone regeneration using outgrowth endothelial cells. *Biomaterials* **2009**, *30* (7), 1329−1338.
(26) Ghanaati, S.; Unger, R. E.; Webber, M. J.; Barbeck, M.; Orth, C.; Kirkpatrick, J. A.; Booms, P.; Motta, A.; Migliaresi, C.; Sader, R. A.; et al. Scaffold vascularization in vivo driven by primary human osteoblasts in concert with host inflammatory cells. *Biomaterials* **2011**, *32* (32), 8150−8160.
(27) Li, J. J.; Kaplan, D. L.; Zreiqat, H. Scaffold-based regeneration of skeletal tissues to meet clinical challenges. *J. Mater. Chem. B* **2014**, *2* (42), 7272−7306.
(28) Karageorgiou, V.; Kaplan, D. L. Porosity of 3D biomaterial scaffolds and osteogenesis. *Biomaterials* **2005**, *26* (27), 5474−5491.
(29) Maraldi, T.; Riccio, M.; Resca, E.; Pisciotta, A.; La Sala, G. B.; Ferrari, A.; Bruzzesi, G.; Motta, A.; Migliaresi, C.; Marzona, L.; et al. Human amniotic fluid stem cells seeded in fibroin scaffold produce in vivo mineralized matrix. *Tissue Eng., Part A* **2011**, *17* (21−22), 2833−2843.
(30) Riccio, M.; Maraldi, T.; Pisciotta, A.; La Sala, G. B.; Ferrari, A.; Bruzzesi, G.; Motta, A.; Migliaresi, C.; De Pol, A. Fibroin scaffold repairs critical-size bone defects in vivo supported by human amniotic fluid and dental pulp stem cells. *Tissue Eng., Part A* **2012**, *18* (9−10), 1006−1013.
(31) Le, T. D. H.; Liaudanskaya, V.; Bonani, W.; Migliaresi, C.; Motta, A. Enhancing bioactive properties of silk fibroin with diatom particles for bone tissue engineering applications. *J. Tissue Eng. Regener. Med.* **2018**, *12*, 89.
(32) Wenk, E.; Merkle, H. P.; Meinel, L. Silk fibroin as a vehicle for drug delivery applications. *J. Controlled Release* **2011**, *150* (2), 128−141.
(33) Mourino, V.; Boccaccini, A. R. Bone tissue engineering therapeutics: controlled drug delivery in three-dimensional scaffolds. *J. R. Soc., Interface* **2010**, *7* (43), 209−227.
(34) Mistry, B. D. *A Handbook of Spectroscopic Data Chemistry*, 20th ed.; Oxford Book Company: Jaipur, India, 2009.
(35) Hu, X.; Kaplan, D.; Cebe, P. Determining beta-sheet crystallinity in fibrous proteins by thermal analysis and infrared spectroscopy. *Macromolecules* **2006**, *39* (18), 6161−6170.
(36) Bucciarelli, A.; Pal, R. K.; Maniglio, D.; Quaranta, A.; Mulloni, V.; Motta, A.; Yadavalli, V. K. Fabrication of Nanoscale Patternable Films of Silk Fibroin Using Benign Solvents. *Macromol. Mater. Eng.* **2017**, *302* (7), 1700110.
(37) Asakura, T.; Okushita, K.; Williamson, M. P. Analysis of the structure of Bombyx mori silk fibroin by NMR. *Macromolecules* **2015**, *48* (8), 2345−2357.
(38) Callone, E.; Dire', S.; Hu, X.; Motta, A. Processing influence on molecular assembling and structural conformations in silk fibroin: elucidation by solid state NMR. *ACS Biomater. Sci. Eng.* **2016**, *2*, 758−767.
(39) Nielsen, M.; Larsen, L. H.; Ottosen, L. D. M.; Revsbech, N. P. Hydrogen microsensors with hydrogen sulfide traps. *Sens. Actuators, B* **2015**, *215*, 1−8.
(40) Manferdini, C.; Gabusi, E.; Grassi, F.; Piacentini, A.; Cattini, L.; Zini, N.; Filardo, G.; Facchini, A.; Lisignoli, G. Evidence of specific characteristics and osteogenic potentiality in bone cells from tibia. *J. Cell. Physiol.* **2011**, *226* (10), 2675−2682.
(41) Stuart, B. *Biological applications of infrared spectroscopy*; Ando, D., Ed.; Published on behalf of ACOL (University of Greenwich) by John Wiley; John Wiley & Sons, Inc.: Chichester, U.K., 1997.
(42) Barth, A. Infrared spectroscopy of proteins. *Biochim. Biophys. Acta, Bioenerg.* **2007**, *1767* (9), 1073−1101.
(43) Iizuka, E.; Yang, J. T. The Disordered and β-conformations of Silk Fibroin in Solution. *Biochemistry* **1968**, *7* (6), 2218−2228.
(44) Zhang, H.; Li, L.-L.; Dai, F.-Y.; Zhang, H.-H.; Ni, B.; Zhou, W.; Yang, X.; Wu, Y.-Z. Preparation and characterization of silk fibroin as a biomaterial with potential for drug delivery. *J. Transl. Med.* **2012**, *10*, 117.
(45) Motta, A.; Fambri, L.; Migliaresi, C. Regenerated silk fibroin films: Thermal and dynamic mechanical analysis. *Macromol. Chem. Phys.* **2002**, *203* (10−11), 1658−1665.
(46) Lu, Q.; Zhang, B.; Li, M.; Zuo, B.; Kaplan, D. L.; Huang, Y.; Zhu, H. Degradation mechanism and control of silk fibroin. *Biomacromolecules* **2011**, *12* (4), 1080−1086.
(47) Motta, A.; Segnana, P.; Verin, L.; La Monica, S.; Fumarola, C.; Bucci, G.; Gussago, F.; Cantoni, A. M.; Ampollini, L.; Migliaresi, C. Physico-chemical characterization and biological evaluation of two fibroin materials. *J. Tissue Eng. Regener. Med.* **2014**, *8* (11), 874−885.
(48) Hughes, M. N.; Centelles, M. N.; Moore, K. P. Making and working with hydrogen sulfide. *Free Radical Biol. Med.* **2009**, *47* (10), 1346−1353.
(49) Olson, K. R. A. Practical Look at the Chemistry and Biology of Hydrogen Sulfide. *Antioxid. Redox Signaling* **2012**, *17* (1), 32−44.
(50) Kolluru, G. K.; Shen, X.; Bir, S. C.; Kevil, C. G. Hydrogen sulfide chemical biology: Pathophysiological roles and detection. *Nitric Oxide* **2013**, *35*, 5−20.
(51) Kim, H. J.; Kim, U. J.; Leisk, G. G.; Bayan, C.; Georgakoudi, I.; Kaplan, D. L. Bone regeneration on macroporous aqueous-derived silk 3-D scaffolds. *Macromol. Biosci.* **2007**, *7* (5), 643−655.
(52) Mi, H. Y.; Jing, X.; Salick, M. R.; Cordie, T. M.; Turng, L. S. Carbon nanotube (CNT) and nanofibrillated cellulose (NFC) reinforcement effect on thermoplastic polyurethane (TPU) scaffolds fabricated via phase separation using dimethyl sulfoxide (DMSO) as solvent. *J. Mech. Behav. Biomed. Mater.* **2016**, *62*, 417−427.
(53) Zhang, X.; Cao, C.; Ma, X.; Li, Y. Optimization of macroporous 3-D silk fibroin scaffolds by salt-leaching procedure in organic solvent-free conditions. *J. Mater. Sci.: Mater. Med.* **2012**, *23* (2), 315−324.
(54) Yao, D.; Dong, S.; Lu, Q.; Hu, X.; Kaplan, D. L.; Zhang, B.; Zhu, H. Salt-leached silk scaffolds with tunable mechanical properties. *Biomacromolecules* **2012**, *13* (11), 3723−3729.
(55) Wilson, D.; Valluzzi, R.; Kaplan, D. L. Conformational transitions in model silk peptides. *Biophys. J.* **2000**, *78* (5), 2690−2701.
(56) Tian, D.; Li, T.; Zhang, R.; Wu, Q.; Chen, T.; Sun, P.; Ramamoorthy, A. Conformations and Intermolecular Interactions in Cellulose/Silk Fibroin Blend Films: A Solid-State NMR Perspective. *J. Phys. Chem. B* **2017**, *121* (25), 6108−6116.
(57) Deleon, E. R.; Stoy, G. F.; Olson, K. R. Passive loss of hydrogen sulfide in biological experiments. *Anal. Biochem.* **2012**, *421* (1), 203−207.

DOI: 10.1021/acsbiomaterials.8b00212
ACS Biomater. Sci. Eng. XXXX, XXX, XXX−XXX